# Chromatin phosphoproteomics unravels a function for AT-hook motif nuclear localized protein AHL13 in PAMP-triggered immunity

Naganand Rayapuram[a,1,2], Mai Jarad[a,b,1], Hanna M. Alhoraibi[c,1], Jean Bigeard[d,e,1], Aala A. Abulfaraj[f], Ronny Völz[g], Kiruthiga Gayathri Mariappan[a], Marilia Almeida-Trapp[a,h], Maria Schlöffel[i], Emmanuelle Lastrucci[j], Ludovic Bonhomme[k], Andrea A. Gust[i], Axel Mithöfer[h], Stefan T. Arold[l], Delphine Pflieger[j,m,n,2], and Heribert Hirt[a,o,2]

[a]Division of Biological and Environmental Sciences and Engineering, King Abdullah University of Science and Technology, Thuwal 23955, Saudi Arabia; [b]Centre for Research in Agricultural Genomics, Consejo Superior de Investigaciones Cientificas, Catalan Institute for Food and Agricultural Research and Technology, Autonomous University of Barcelona, University of Barcelona, 08007 Barcelona, Spain; [c]Department of Biochemistry, Faculty of Science, King Abdulaziz University, 21551 Jeddah, Saudi Arabia; [d]CNRS, Institut National de Recherche pour l'Agriculture, l'Alimentation, et l'Environnement, University Evry, Institute of Plant Sciences Paris-Saclay, Université Paris-Saclay, 91405 Orsay, France; [e]Institut National de Recherche pour l'Agriculture, l'Alimentation, et l'Environnement, Institute of Plant Sciences Paris-Saclay, Université de Paris, CNRS, 91405 Orsay, France; [f]Department of Biological Sciences, College of Sciences and Arts-Rabigh Campus, King Abdulaziz University, 21589 Jeddah, Saudi Arabia; [g]Plant Immunity Research Center, Seoul National University, 08826 Seoul, Korea; [h]Research Group Plant Defense Physiology, Max Planck Institute for Chemical Ecology, 07745 Jena, Germany; [i]Center for Plant Molecular Biology, Eberhard-Karls-Universität Tübingen, 72074 Tübingen, Germany; [j]Commissariat à l'Energie Atomique, INSERM, Interdisciplinary Research Institute Grenoble, Large Scale Biology Laboratory, University Grenoble Alpes, 38000 Grenoble, France; [k]Institut National de Recherche pour l'Agriculture, l'Alimentation, et l'Environnement, Laboratoire de Génétique, Diversité, Ecophysiologie des Céréales, Université Clermont Auvergne, 63000 Clermont Ferrand, France; [l]Computational Bioscience Research Center, Division of Biological and Environmental Sciences and Engineering, King Abdullah University of Science and Technology, Thuwal 23955-6900, Saudi Arabia; [m]Interdisciplinary Research Institute of Grenoble, Large Scale Biology Laboratory, CNRS, F-38000 Grenoble, France; [n]CNRS, LAMBE UMR 8587, Université d'Evry Val d'Essonne, 91000 Evry, France; and [o]Max Perutz Laboratories, University of Vienna, 1030 Vienna, Austria

Edited by Cyril Zipfel, University of Zurich, Zurich, Switzerland, and accepted by Editorial Board Member Sheng Yang He November 30, 2020 (received for review March 16, 2020)

**In many eukaryotic systems during immune responses, mitogen-activated protein kinases (MAPKs) link cytoplasmic signaling to chromatin events by targeting transcription factors, chromatin remodeling complexes, and the RNA polymerase machinery. So far, knowledge on these events is scarce in plants and no attempts have been made to focus on phosphorylation events of chromatin-associated proteins. Here we carried out chromatin phosphoproteomics upon elicitor-induced activation of *Arabidopsis*. The events in WT were compared with those in *mpk3*, *mpk4*, and *mpk6* mutant plants to decipher specific MAPK targets. Our study highlights distinct signaling networks involving MPK3, MPK4, and MPK6 in chromatin organization and modification, as well as in RNA transcription and processing. Among the chromatin targets, we characterized the AT-hook motif containing nuclear localized (AHL) DNA-binding protein AHL13 as a substrate of immune MAPKs. *AHL13* knockout mutant plants are compromised in pathogen-associated molecular pattern (PAMP)-induced reactive oxygen species production, expression of defense genes, and PAMP-triggered immunity. Transcriptome analysis revealed that *AHL13* regulates key factors of jasmonic acid biosynthesis and signaling and affects immunity toward *Pseudomonas syringae* and *Botrytis cinerea* pathogens. Mutational analysis of the phosphorylation sites of AHL13 demonstrated that phosphorylation regulates AHL13 protein stability and thereby its immune functions.**

phosphoproteomics | MAPK signaling | chromatin | immunity | AT-hook motif transcription factor

Signaling of a wide variety of factors is mediated via the sequential phosphorylation and activation of mitogen-activated protein kinase (MAPK) pathways. MAPK pathways are minimally constituted of MAPK kinase kinases (MAPKKKs), which activate MAPK kinases (MAPKKs) and in turn MAPKs. Activated MAPKs phosphorylate their substrates on serine or threonine residues of (S/T)P motifs, and this posttranslational modification may regulate protein activity, subcellular localization, or stability. The partitioning of MAPKs to various compartments and cellular structures allows substrate-specific interactions and responses (1). One of the most prominent responses to MAPKs occurs at the chromatin level. Besides ample evidence of transcription factors as direct MAPK targets (2, 3), there is evidence that MAPKs can directly interact with promoters (4). Moreover, MAPKs can activate other protein kinases to modify histones, as shown by the MAPK-targeted MSKs, which phosphorylate histone H3 at S10 and S28, thereby modifying nucleosomes in the nearby promoters (5).

The SWI/SNF family of chromatin remodeling complexes modulates transcription by changing the accessibility of genes to transcription factors and the transcriptional machinery (6). In yeast, the recruitment of osmotic stress-activated Hog1 MAPK to the SWI/

## Significance

Mitogen-activated protein kinases (MAPKs) function in all eukaryotes in signaling extracellular stimuli to intracellular responses and ultimately link them to chromatin events by targeting transcription factors and chromatin remodeling complexes. In plants, MAPKs play crucial roles in immunity, development, and stress responses, but so far no attempts have been made to identify phosphorylation of chromatin-associated proteins. By using a phosphoproteomic approach on MAPK mutants, we identified a number of chromatin-associated MAPK substrates and characterize an AT-hook motif containing nuclear localized (AHL) DNA-binding protein 13 in plant immunity and demonstrate that phosphorylation regulates AHL13 protein stability and, in turn, its function in response to pathogens.

Author contributions: N.R., J.B., D.P., and H.H. designed research; N.R., M.J., H.M.A., J.B., A.A.A., R.V., M.A.-T., M.S., and D.P. performed research; N.R., J.B., K.G.M., E.L., L.B., A.A.G., A.M., S.T.A., D.P., and H.H. analyzed data; and N.R., H.M.A., J.B., S.T.A., D.P., and H.H. wrote the paper.

The authors declare no competing interest.

This article is a PNAS Direct Submission. C.Z. is a guest editor invited by the Editorial Board.



[1]N.R., M.J., H.M.A., and J.B. contributed equally to this work.

[2]To whom correspondence may be addressed. Email: naganand.rayapuram@kaust.edu.sa, Delphine.PFLIEGER@cea.fr, or heribert.hirt@kaust.edu.sa.

This article contains supporting information online at https://www.pnas.org/lookup/suppl/doi:10.1073/pnas.2004670118/-/DCSupplemental.

Published January 8, 2021.

SNF remodeling complex results in the eviction of nucleosomes, allowing efficient transcription of the targeted promoters (7). Moreover, MAPKs not only interact to promoter regions through transcription factors or chromatin remodeling complexes, but can also interact directly with the elongating RNA polymerase complex, as seen for Hog1 on its target genes (8). The localization of MAPKs is not only important for transcription factor activation and histone modification, but also for the negative regulation of the upstream kinases, as seen for the *Drosophila* MAPK JNK (9). From these studies, it appears that recruitment of MAPKs to chromatin is widely conserved in all eukaryotes, but knowledge in plants is so far lacking.

In plants, MAPK pathways are implicated in development, biotic, and abiotic stress (10–12). Among these, MPK3, MPK4, and MPK6 have been studied extensively due to their involvement in many of these processes, such as cold tolerance, where MPK4 is a positive and MPK3/MPK6 are negative regulators (13–15). Among other roles, MPK4 is also involved in microtubule organization, cytokinesis, and pollen development (16–18), MPK3 plays a role in leaf development, MPK6 in shoot branching (19), and MPK3 and MPK6 both determine stomatal development and patterning (20, 21). MAPKs also play an important role in plant immunity. Pathogen-associated molecular patterns (PAMPs) are recognized by plant pattern-recognition receptors leading to PAMP-triggered immunity (PTI) (22). To overcome plant defense, pathogens developed effectors to counteract PTI that resulted in effector-triggered susceptibility. Resistant plant varieties recognize some of these effectors by resistance proteins (R proteins) leading to effector-triggered immunity (ETI) (23). PTI and ETI trigger callose deposition to strengthen the cell walls (24) and the synthesis of antimicrobial compounds, like the phytoalexin camalexin and pathogenesis-related proteins (25, 26). One prominent PAMP is the flg22 peptide from the flagellin of *Pseudomonas aeruginosa*. Flg22 is recognized by the FLS2 receptor complex (27) and activates several MAPKs, including MPK3, MPK4, and MPK6 (28–30), which are part of two MAPK modules MAPKKK3/MAPKKK5-MKK4/MKK5-MPK3/MPK6 (31) and MEKK1-MKK1/MKK2-MPK4 (32, 33). Previously, we determined the specific and cooperative roles of MPK3, MPK4, and MPK6 in transcriptional reprogramming during PTI (29).

Several large-scale in vivo approaches using phosphoproteomics have identified MAPK candidate substrates in plants (34–37). Nonetheless, these studies were performed from total protein extracts or enriched cytoplasmic fractions, but not from chromatin. To investigate chromatin targets of MPK3, MPK4, and MPK6, we quantitatively compared the chromatin phosphoproteomes of WT and *mpk3*, *mpk4*, and *mpk6* mutants with and without PAMP treatment. Overall, we identified 56 differentially phosphorylated peptides, of which 38 possessed (S/T)*P sites, designating them as potential MPK3, MPK4, or MPK6 substrates. One of the chromatin-associated proteins that showed differential phosphorylation by MAPKs is the AT-hook motif containing nuclear localized protein 13 (AHL13). The *AHL* gene family is conserved across land plant species and the genome of *Arabidopsis* codes for 29 *AHL* genes (38–43). AHL proteins have been shown to play a role in plant growth, development, and differentiation, including axillary meristem maturation for AHL15, root system architecture for AHL18, flowering for AHL22, and petiole growth for AHL27 and AHL29 (44–51). AHLs have also been shown to regulate hormones, with AHL15 and AHL25 regulating gibberellic acid biosynthesis, and AHL27 and AHL29 regulating auxin biosynthesis (49, 52, 53). While AHL19 and AHL20 have been implicated in immunity, AHL10 was shown to regulate growth regulation during water limitation stress (54–56). AHL proteins are phylogenetically divided into clades A and B, but all contain two conserved structural domains: One or two AT-hook–like motifs mediate binding to AT-rich DNA regions, and one plant and prokaryote conserved (PPC) domain is essential for AHL nuclear localization and allows interaction of AHLs with each other and other nuclear proteins to form homo- and hetero-multimers (57). In this study we show that clade B AHL13 is a substrate of MAPKs and *AHL13* loss-of-function mutant plants are compromised in their response to bacterial and fungal pathogens. Using stable *Arabidopsis* lines expressing the phosphodead and phosphomimic mutant versions of AHL13, we show that the AHL13 phosphorylation results in the stabilization of the protein to regulate plant immunity.

## Results

**Analysis of Chromatin Phosphoproteomes.** To identify chromatin-associated phosphorylation events, we performed a phosphoproteomic analysis of chromatin proteins isolated from WT Col-0 and *mpk3*, *mpk4*, or *mpk6* mutant plants with and without a 15-min treatment with 1 μM flg22. At least three independent biological repeats were performed. Chromatin-associated proteins were purified from nuclei by high salt extraction and phosphopeptides were then enriched by immobilized metal affinity chromatography (IMAC) before identification by liquid chromatography-tandem mass spectrometry (LC-MS/MS) (Fig. 1*A*). Overall, we identified 336 phosphopeptides, corresponding to 234 phosphoproteins (Dataset S1). Fig. 1*B* shows the distribution of singly, doubly, triply, and multiply modified phosphopeptide sequences. The phosphopeptides with precise modification sites distributed into 76.8% Ser, 19.9% Thr, and 3.3% Tyr phosphorylated residues (Fig. 1*C*). A number of phosphorylation motifs were identified by motif-x analysis (58) (Fig. 1*D*). The low-stringency (S/T)*P MAPK motif accounted for the largest peptide population, followed by acidophilic motifs showing S(D/E)x(D/E), with "x" frequently being a D or E.

The effect of flg22 treatment, the consequence of *MAPK* mutations and their combined impact on protein phosphorylation patterns were assessed by two-way ANOVA analysis (*Experimental Procedures*, Fig. 1 *E* and *F*, and *SI Appendix*, Fig. S1). By computing the significance of the variance driven by each factor, the phosphorylation events were categorized into three main groups: 1) Those that depend on *MAPK* mutation only (*MAPK*-dependent variations), 2) those specifically associated to PAMP-induced responses (flg22-induced changes), and 3) those that are flg22-induced and at the same time *MAPK*-dependent (see *SI Appendix*, Fig. S1 for a flowchart for details on the analysis and statistics).

A substantial number of proteins were verified to be nuclear or chromatin-associated in other studies and databases, but many were novel. This is probably due to the fact that our dataset comes from PAMP-treated samples and besides, there is no robust reference set for chromatin proteins. We further compared the MAPK targets that we identified to those reported in prior large-scale in vivo studies (Fig. 1*G*). Although these were all phosphoproteomic studies focusing on MPK3, MPK6, and eventually MPK4, our work is the only one focusing on chromatin while the other reports analyzed total protein extracts or enriched cytoplasmic fractions (34, 37). Although no overlap was identified with the work of Huck et al. (35), a limited overlap of putative MAPK substrates was identified in these various studies (34, 37) (Fig. 1*G* and Dataset S2), underscoring that subcellular phosphoproteomics, such as done here with chromatin, holds a great potential to identify novel candidate MAPK substrates.

**MAPK Chromatin Targets with Potentially Nonimmune Functions.** We previously found that *mpk3*, *mpk4*, and *mpk6* mutants show massive changes in gene expression under ambient growth conditions, confirming a role of these MAPKs in nonimmune functions (29). From the ANOVA tests performed, we identified 42 proteins from 50 phosphopeptides whose phosphorylation status was dependent on 1 of the 3 MAPKs; more precisely, 12 of them were detected by 13 phosphopeptides not affected by flg22-treatment (Fig. 2 *A* and *B* and Datasets S3 and S4). The vast majority of the 42 proteins showed reduced phosphorylation levels in any of the *mpk3*, *mpk4*,

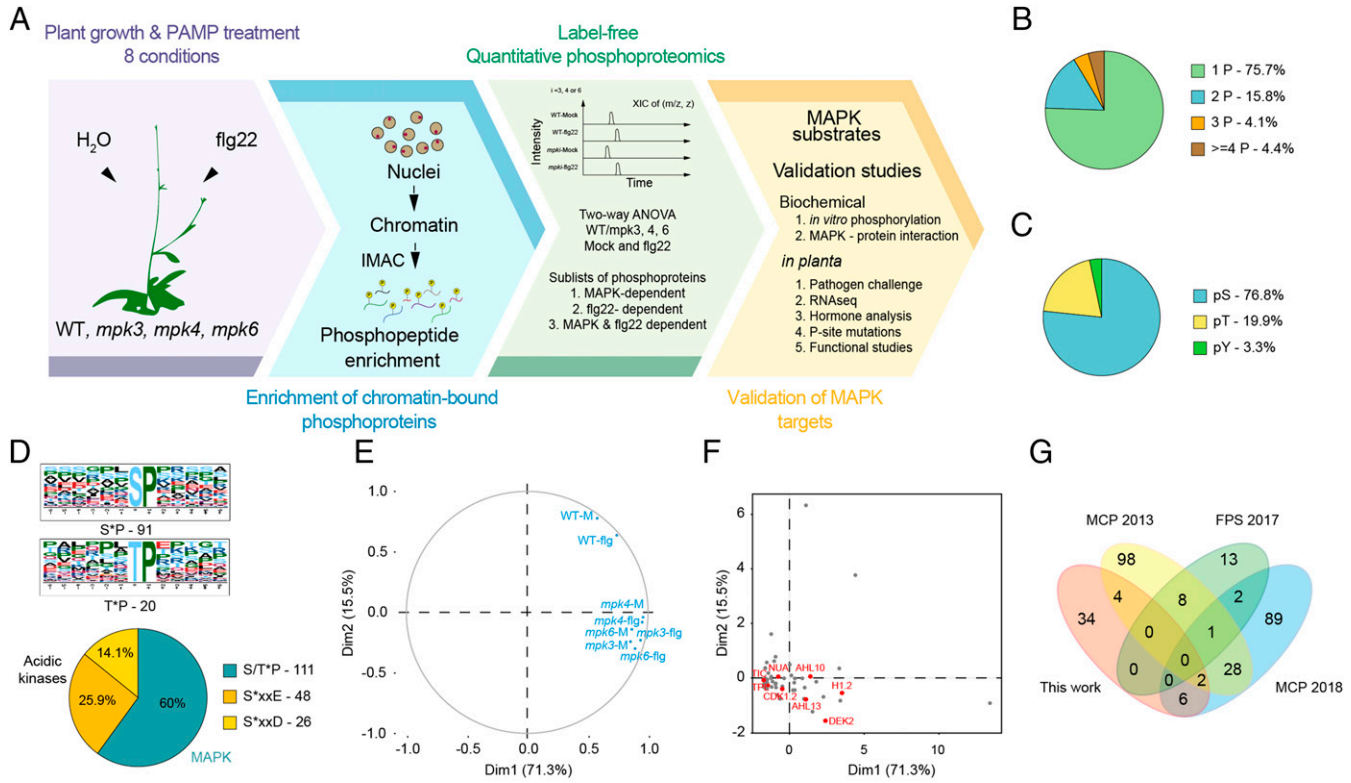


**Fig. 1.** Phosphoproteomics experimental workflow and data analysis. (*A*) Schematic representation of the phosphoproteomics experimental workflow and data analysis for the identification of MAPK substrates. Phosphopeptides were enriched using IMAC from WT plants and *mpk3*, *mpk4*, and *mpk6* mutants treated with and without flg22 and analyzed by LC-MS/MS. Database searches were carried out using the program Mascot and phosphosite localization was ascertained using FragMixer. Relative quantification was carried out using MassChroQ, followed by statistical analysis of quantitative data to highlight sequences whose abundance was significantly modulated. The list of identified phosphopeptides was subjected to motif analysis using motif-x. (*B*) Number of phosphorylation sites per peptide. (*C*) Distribution of phosphorylated amino acids. (*D*) Motifs enriched by motif-x. (*E*) Principal component analysis of the identified phosphopeptides across the eight conditions. (*F*) Principal component analysis of a few candidate proteins are highlighted. (*G*) Venn diagram showing the overlap of candidate proteins identified in this study with other relevant studies (34, 35, 37).

or *mpk6* mutants. Among these, 32 phosphopeptides possessed 1 or 2 (S/T)*P motifs, 10 an acidophilic motif [e.g., S*(D/E) or S*X(D/E)], and 14 the motif (K/R)XX(S/T)*. The absence or reduction of phosphorylation in a single *MAPK* mutant but not in WT or the other *MAPK* mutants constituted evidence for their direct or indirect regulation by a given MAPK. In this way, we identified the transcriptional regulator Topless (TPL) to be a substrate of MPK3 at AP(s)*PVNNPLLGGIPK. We also found that MPK6 targets the transcription factor BIN4 at TEDKDTDTTIAEQVTPEK(s)*PK, the nuclear pore anchor NUA at VPSSTPLIK(s)*PVATTQQLPK and AP(s)*PGGGSSTIVTLADR, and the AT-hook protein AHL10 (AT2G33620) at VAPTQVLMTPS(s)*PQSR.

In agreement with the partially redundant functions of two or all three MAPKs (29), single and dual phosphorylation of SPEKEEVQPETLA(t)*PTQ(s)*PSR of NUA was diminished in *mpk3* or *mpk6* mutants. Lack of MPK3 and MPK6 was seen to compromise phosphorylation of the chromatin-associated regulator Time for Coffee (TIC) at S(sPsPAPVs)*PLVSTWK. The lack of either MPK3, MPK4, or MPK6 dramatically compromised (by more than a factor of 40) phosphorylation of the transcription factor WRKY20 at ILLPEP(sPtt)*GSLFKPRPVHISASSSSYTGR. However, these results cannot be easily ascribed to this site being a shared target of MPK3, MPK4, or MPK6 and several tentative mechanisms can be proposed: A cooperative effect between MAPKs, a multimeric effect (formation of MAPK heterodimers), or an indirect genetic effect (e.g., increased phosphatase activity) might be responsible for this observation, which requires further investigation.

Finally, in some cases, we also observed increased phosphorylation levels in a given MAPK mutant when compared to WT plants. This was evident for the DEK domain-containing chromatin-associated protein AT5G63550 in *mpk3* or the leucine-rich repeat protein kinase AT3G02880 in *mpk6* mutants. Interestingly, in *mpk4* mutants, histone H1.2, NUA [at RAP(s)*PGGGSSTIVTLADR], CDK-activating kinase 4 (AT1G66750), AT5G47690, and AT5G66540 showed higher phosphorylation levels than in WT.

**Analysis of PAMP-Induced Changes of Chromatin Protein Amounts in WT and *mapk* Mutants.** Since several hundred genes are differentially expressed in *mpk3*, *mpk4*, and *mpk6* (29), it was important to distinguish between changes in phosphorylation and changes in protein amounts. We thus performed LC-MS/MS analyses of the nonphosphorylated peptides, which were not retained on the IMAC resin (Dataset S5). As expected, of the 322 protein families quantified in the chromatin samples, the abundance of 54 proteins varied among WT and *mpk3*, *mpk4*, and *mpk6* mutants ($P < 0.01$). Five proteins showed abundance variations between genotypes and upon flg22 treatment (genotype x treatment effect). However, none of the protein levels changed significantly upon 15-min flg22 treatment in WT plants ($P < 0.01$), indicating that PAMP-induced phosphorylation does not lead to major changes in protein abundance or stability in the initial few minutes after flg22 treatment.

**PAMP-Induced Chromatin Phosphorylation Targets and Role of MAPKs.** To identify proteins involved in immunity, we looked for peptides

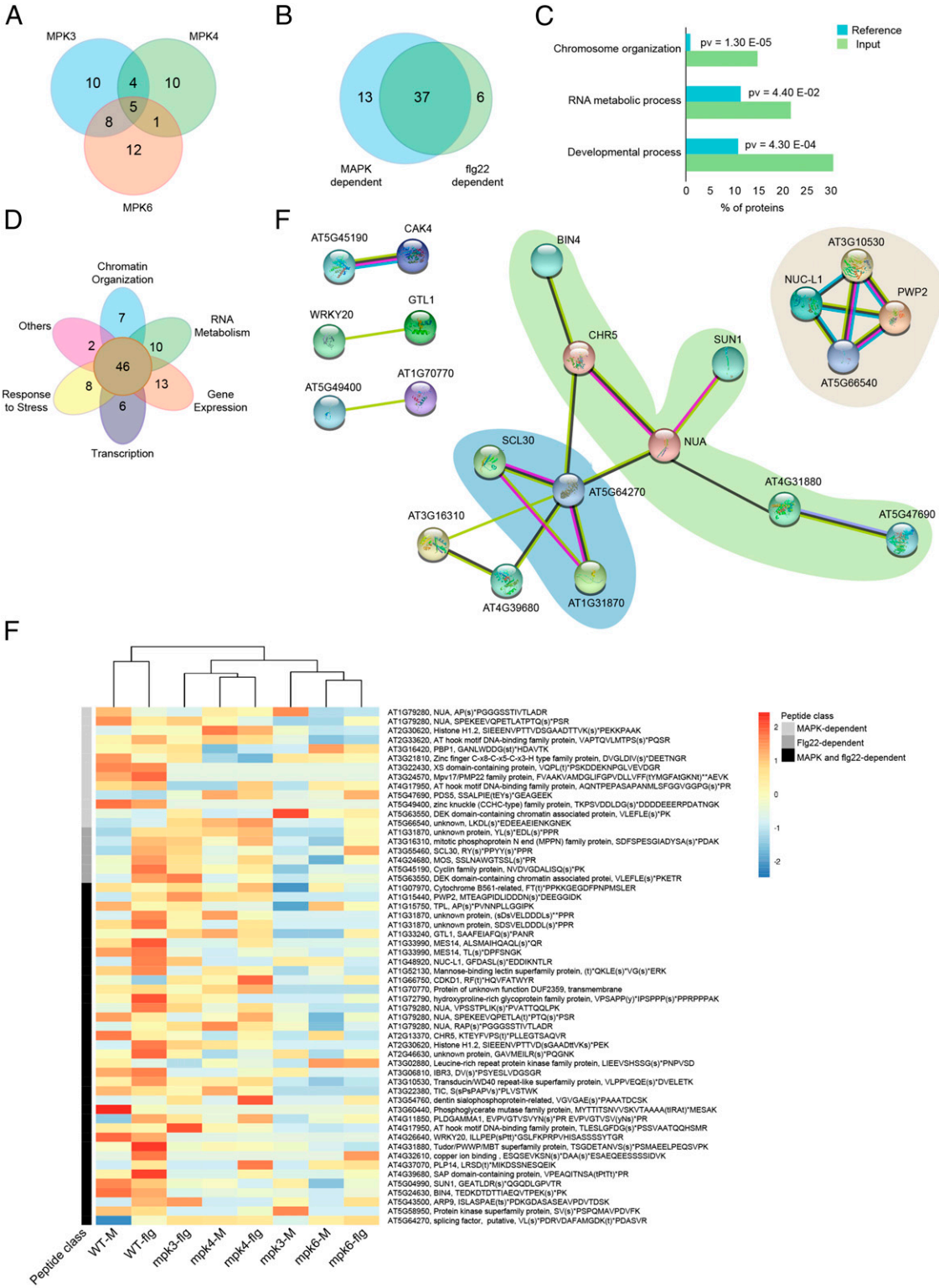


**Fig. 2.** Overview of the chromatin phosphoproteome. (*A*) Venn diagram showing specific and shared targets of MPK3, -4, and -6. (*B*) Venn diagram depicting MAPK-dependent and flg22-dependent phosphopeptides. (*C*) GO enrichment of the phosphopeptides into three relevant categories. (*D*) Flower plot diagram with the central circle showing the 46 proteins and each petal showing the different categories of proteins, chromosome organization, RNA metabolism, gene expression, transcription, response to stress, and other biological processes. (*E*) Targets for MPK3, -4, and -6 were pooled and used to generate a network using STRING (v10.0) within the Cytoscape environment. Clusters with targets involved in RNA metabolic processes and splicing are highlighted in beige and blue, respectively. Phosphoproteins involved in nuclear structure and chromosome organization are highlighted in pale green. (*F*) The heatmap showing the relative abundances of phosphopeptides significantly affected in WT and *mapk* mutants with or without flg22 treatment was computed from scaled and centered values.

whose phosphorylation levels changed upon flg22 treatment. By two-way ANOVA, a total of 43 phosphopeptides, corresponding to 38 proteins, were identified (Datasets S3 and S4). Ten proteins were de novo-phosphorylated in WT plants after PAMP treatment. Among them, ARP9 was detected by ISLASPAE(ts)*PDKGDASASEAVPDVTDSK, whose phosphorylation was only impaired upon PAMP treatment in the *mpk4* mutant, indicating that this SP site is specifically targeted by MPK4. Although the phosphorylation of several proteins was compromised in one or more MAPK mutants, phosphorylation was often possible upon PAMP treatment. For example, modifier of SNC1 (MOS1) and BIN4 are not phosphorylated in *mpk6*, but get phosphorylated after flg22 treatment. These data indicate that MPK3, MPK4, or MPK6 are redundantly involved in the phosphorylation of these substrates. Alternatively, other PAMP-induced MAPKs—such as MPK1, MPK11, or MPK13 (30) —or other proline-directed protein kinases, such as some CDKs (cyclin-dependent protein kinases), could also be responsible for the PAMP-induced phosphorylation of these targets.

**MAPK Docking Sites in the Differentially Phosphorylated Proteins.** The interaction of MAPKs with their substrates is usually facilitated by the presence of one or more MAPK docking sites (D-sites) (59). We thus searched for the presence of D-sites in the phosphoproteins using the ELM program (Dataset S3). Of the 30 candidate MAPK-targeted proteins, harboring an (S/T)*P site, 4 had 1, 22 multiple, and 4 no known D-sites. Chromatin-remodeling factor 5 (CHR5; AT2G13370) had the greatest number of D-sites.

**Chromatin Phosphoproteome, Gene Ontology Analyses, and Interaction Network.** In order to understand the role of the phosphoproteins in gene regulation, we collated the chromatin phosphoproteomes from the various comparisons and obtained 56 phosphopeptides whose phosphorylation was either up- or down-regulated in a particular *mapk* mutant or after flg22 treatment. Of the 56 phosphopeptides that change in their phosphorylation state, a Venn diagram shows that 13 depend only on either MPK3, MPK4, or MPK6, 6 change upon flg22-treatment independently of the 3 MAPKs, and for 37 peptides, the change in phosphorylation is induced by flg22 but also requires functional MPK3, MPK4, or MPK6 (Fig. 2*B*). The gene ontology (GO) enrichment categories of the combined chromatin phosphoproteomes correspond to chromosome organization, RNA metabolic, and developmental processes (Fig. 2*C*). The different categories of proteins are described in a flower plot diagram with the central circle showing the 46 proteins (56 phosphopeptides) that are involved in processes from chromosome organization, RNA metabolism, gene expression, transcription, response to stress, and other biological processes (Fig. 2*D*).

Next, we analyzed the three MAPK-dependent phosphoproteomes for protein interaction networks using the program STRING (60) within the Cytoscape environment (Fig. 2*E*). These interaction networks and GO analyses showed a common role of MPK3, MPK4, and MPK6 in RNA processing/metabolism (Fig. 2*E*, beige), chromosome organization (Fig. 2*E*, pale green), and RNA splicing (Fig. 2*E*, blue).

We next generated a heat map (Fig. 2*F*) of the 56 phosphopeptides whose phosphorylation levels changed either upon flg22 treatment, in any of the *MAPK* mutants without flg22 treatment or whose flg22-induced changes were linked to any of the three MAPKs: MPK3, MPK4, or MPK6. In addition to observing that most proteins show reduced phosphorylation levels in specific *MAPK* mutants, some proteins showed increased phosphorylation levels, suggesting that the MAPKs might also regulate other processes, including the activation of phosphatases, or the de novo synthesis or degradation of specific proteins.

**Phosphorylation of the Transcription Factor AHL13.** Among the *MAPK*-dependent targets, we chose the transcription factor AHL13 (AT4G17950) for further analysis due to the fact that it was phosphorylated at two positions: S109 [TLESLGFDG(s109)*PSSVAATQQHSMR] and S376 [AQNTPEPASAPANMLSFGGVGGPG(s376)*PR]. AHL13 contains two AT-hook motifs in the N terminus and a domain of unknown function (DUF296/PPC) located at the C terminus. $AHL13^{S109}$ is localized before the AT-hook domains and $AHL13^{S376}$ is adjacent to the DUF296/PPC domain of the protein. AHL13 also harbors a predicted D-site located in the DUF296/PPC domain (Fig. 3*A*). Several in vivo phosphoproteomic studies also identified phosphorylation at S109 and S376 of AHL13 (34, 61–63). Compared to WT, S109 phosphorylation levels were reduced in both *mpk3* and *mpk6* mutants. No flg22-induced phosphorylation of AHL13 was observed in WT plants at S109, but phosphorylation strongly increased in flg22-treated *mpk3* mutant plants (Fig. 3*B* and Dataset S3). In addition, phosphorylation of AHL13 at S376 was recently reported to be induced in vivo after a 30-min flg22 treatment (62). However, we only observed a small flg22-induced increase in our data, and a clear role of MAPKs in this process was not evident in the three mutants (Fig. 3*C*).

The phosphoproteomic analysis indicated that the phosphorylation of AHL13 at S109 and S376 depend on MPK3 (Fig. 3 *B* and *C*). However, these data do not distinguish between a direct or indirect mechanism, in which case a MPK3-regulated protein kinase would target S109 or S376. To distinguish between these possibilities, we performed in vitro kinase assays with recombinant AHL13 and constitutively active MPK3, MPK4, and MPK6 proteins before analysis by MS. We found that AHL13 can be phosphorylated at S109 and S376 by MPK3, MPK4, and MPK6 (Fig. 3*D* and *SI Appendix*, Fig. S2).

In order to test the interaction between AHL13 and MPK3, MPK4, and MPK6 in vivo, we performed bimolecular fluorescence complementation assays (BiFC) by coexpressing the proteins transiently in leaf epidermal cells of *Nicotiana benthamiana*. We found that AHL13 interacts exclusively with MPK6 but not with MPK3 and MPK4 (Fig. 3*E* and *SI Appendix*, Fig. S3). In vitro Glutathione S-transferase (GST) pull-down assays between His-MBP-tagged AHL13 and GST-tagged MPK3, MPK4, and MPK6 showed preferential interaction of AHL13 with MPK6 (Fig. 3*F*). Interestingly, we previously showed that *mpk3* mutant plants exhibit higher and longer activation of MPK4 and MPK6 in response to flg22 treatment (29). It is thus possible that the enhanced phosphorylation levels at AHL13 S109 in the flg22-treated *mpk3* mutant is actually due to the enhanced activation of MPK6 or MPK4. Overall, these phosphorylation and interaction data strongly support the hypothesis that AHL13 is a direct MAPK target as suggested in a recent search for MAPK substrates (34).

**PTI Responses Are Compromised in *ahl13* Plants.** To understand the role of AHL13 in PAMP-triggered immune responses and plant immunity, we obtained a T-DNA insertion line *ahl13-1* (SALK_014014). We determined the T-DNA insertion site and showed by qRT-PCR that *AHL13* expression in *ahl13-1* is disrupted (Fig. 4 *A*–*C*). In the *ahl13-1* background, we generated an overexpression line (*ahl13-1 Pro35S::AHL13-GFP*) (OE2) with expression levels of *AHL13* almost 10-fold higher than WT plants, and a complementation line (*ahl13-1 Pro35S::AHL13-GFP*) (C8) with expression levels similar to WT plants (*SI Appendix*, Fig. S4). With the exception of *ahl13-1*, which showed a slight reduction in overall size, C8 and OE2 exhibited a WT phenotype in growth and development (Fig. 4*D*).

We first examined flg22-induced reactive oxygen species (ROS) production, as it is one of the earliest immune responses following PAMP perception. Compared to WT, *ahl13-1* plants were compromised in flg22-induced ROS production, while C8 and OE2 showed comparable ROS production to WT plants (Fig. 4*E*). We then analyzed whether *AHL13* affects PAMP-induced transcription of known PTI marker genes. As revealed by qRT-PCR analyses, basal transcript levels of *FLS2* and *FRK1* were similar in *ahl13-1*

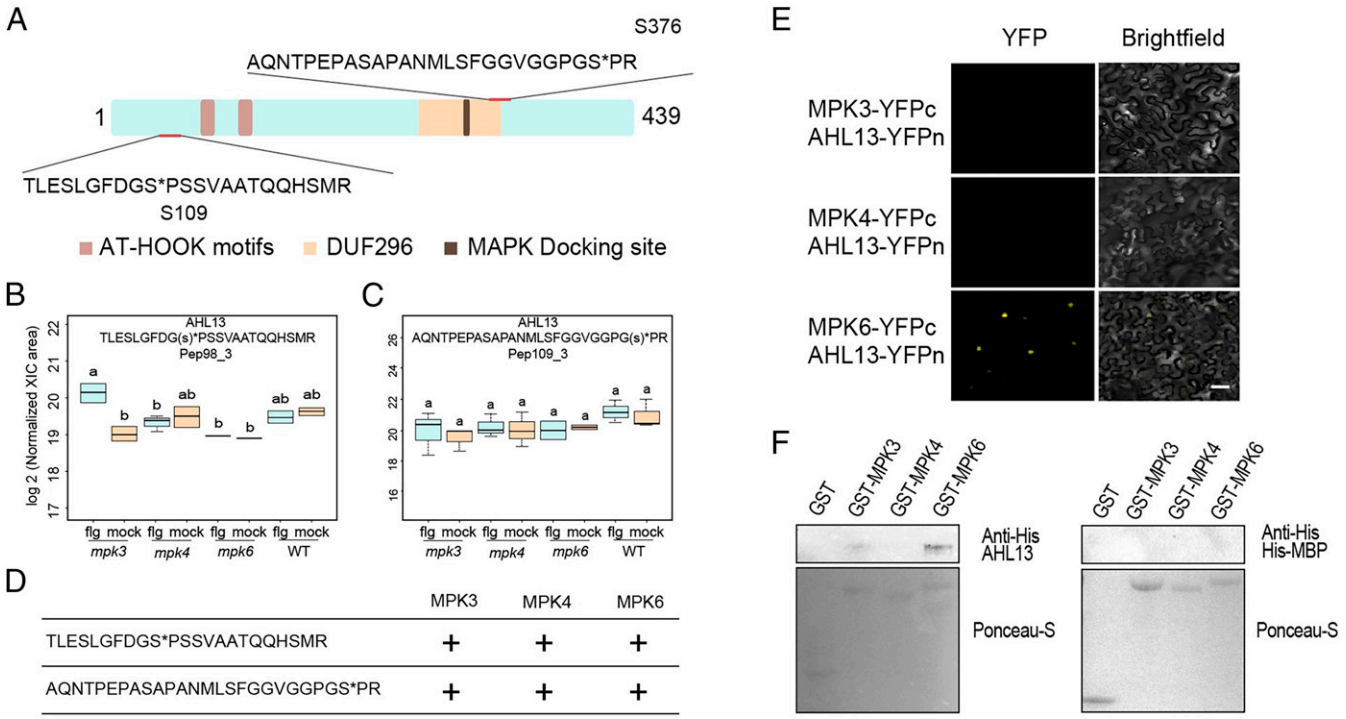


**Fig. 3.** AHL13 protein domains, MAPK phosphorylation and interaction with AHL13. (*A*) Schematic representation showing the AT-hook domains, the DUF296/PPC domain and the MAPK docking site of AHL13. The position of the phosphopeptides is indicated by a red line and phosphosites with an asterisk. (*B* and *C*) Box plots showing the relative abundance of the two phosphopeptides in the eight conditions. (*D*) Results of the phosphorylation of the two phosphosites by the three MAPKs in vitro. (*E*) BiFC analysis of AHL13 with MPK3, MPK4, and MPK6 in *N. benthamiana* leaf epidermal cells. YFP fluorescence was observed by laser-scanning confocal microscopy. (Scale bar, 20 μm.) (*F*) GST pull-down assays were performed by incubating bacterial lysates of GST-tagged MAPKs with GST beads followed by incubation with bacterial lysates His-MBP–tagged AHL13. The pull-downs were probed with anti-His antibody (Western blot: anti-His) and the proteins were stained with Ponceau-S. A negative control for binding of His-MBP with the three MAPKs was carried out in parallel. Letters a, b, and ab are used to show statistically significant differences between variables. For all variables with the same letter, the difference between the means is not statistically significant. If two variables have different letters, they are significantly different.

and WT in untreated plants, but *ahl13-1* was completely inert to flg22-induced expression of the two defense marker genes. In contrast, flg22-induced expression levels of *FLS2* and *FRK1* were similar to WT in C8 and OE2 lines (Fig. 4*F*).

Next, we investigated the role of *AHL13* in plant immune responses upon challenge with the bacterial hemibiotroph *Pseudomonas syringae*. When we challenged the *ahl13* mutant plants with the WT *Pst DC3000* strain and with *Pst DC3000 delta avrPto/avrPtoB*, we did not observe a pathogen phenotype (*SI Appendix*, Fig. S5). We spray-inoculated *ahl13-1* plants with the nonvirulent pathogen strain *P. syringae* pv. *tomato* DC3000 *hrcC*$^{-}$ (*Pst hrcC*$^{-}$), which is used to study PTI as it lacks the type III-secretion system for injecting protein effectors into the host. We observed enhanced susceptibility of the *ahl13-1* mutant compared to WT plants 72 h postinoculation. The enhanced susceptibility phenotype in *ahl13-1* plants was restored to WT levels in the C8 complementation line, but enhanced resistance was observed in the OE2 line (Fig. 4*G*). Cumulatively, these data indicate that *AHL13* is involved in regulating disease resistance to bacterial pathogens.

***AHL13* Regulates *Pst hrcC*$^{-}$-Induced Immune Genes.** In order to understand the role of *AHL13* in regulation of gene expression and plant defense, we performed a global transcriptome analysis of the *ahl13-1* mutant after *Pst hrcC*$^{-}$ infection. RNA was extracted for transcriptome analysis from three independent biological repeats of 14-d-old seedlings of WT and *ahl13-1* mutant plants at 24 h after *Pst hrcC*$^{-}$ or mock treatment.

Compared to WT, *ahl13-1* mock-treated mutant plants showed 1,192 differentially expressed genes (DEGs) with a fold-change > 2 and a $P < 0.05$, of which 518 were up- and 674 down-regulated (Dataset S6). Next, the transcriptome of *ahl13-1* was compared with WT plants following *Pst hrcC*$^{-}$ treatment. *Pst hrcC*$^{-}$ treatment induced the expression of 461 genes and repressed the expression of 262 genes in WT plants, while the expression of 645 genes was induced and 147 genes repressed in the *ahl13-1* mutant plants. Compared to WT plants, 589 of the *ahl13-1 Pst hrcC*$^{-}$-regulated genes were up-regulated, whereas 616 were down-regulated (Dataset S6).

GO analysis of *Pst hrcC*$^{-}$-induced genes exhibited enrichment in genes involved in response to jasmonic acid (JA), secondary metabolic processes, glucosinolate biosynthetic, and metabolic processes. To gain a better understanding of the genes affected by *AHL13* depletion, we carried out hierarchical clustering analysis of *Pst hrcC*$^{-}$-induced genes followed by GO enrichment analysis (Fig. 5*A* and *SI Appendix*, Fig. S6). Clusters 1 and 4 contained the largest number of 552 and 633 DEGs, respectively. The genes in cluster 1 are involved in defense response, response to JA and glucosinolate metabolism, and were highly up-regulated in *ahl13-1* after *Pst hrcC*$^{-}$ treatment compared to WT plants (Fig. 5 *B* and *C*). Cluster 4 genes were nonresponsive to *Pst hrcC*$^{-}$ treatment in *ahl13-1* and enriched in GO terms response to stress, response to stimulus, and hormone-mediated signaling pathway (Fig. 5 *B* and *C*). In order to validate the RNA-sequencing (RNA-seq) results, we carried out qRT-PCR on several of these genes. We observed differential up-regulation of the JA-related marker genes *PDF1.2b* and *VSP2* after treatment with *Pst hrcC*$^{-}$ in *ahl13-1* when compared to WT plants (Fig. 5*D*). The expression of the salicylic acid (SA)-related genes *PR1* and *EDS1* was repressed under these conditions (Fig. 5*D*). Recovery of the expression levels of all of these

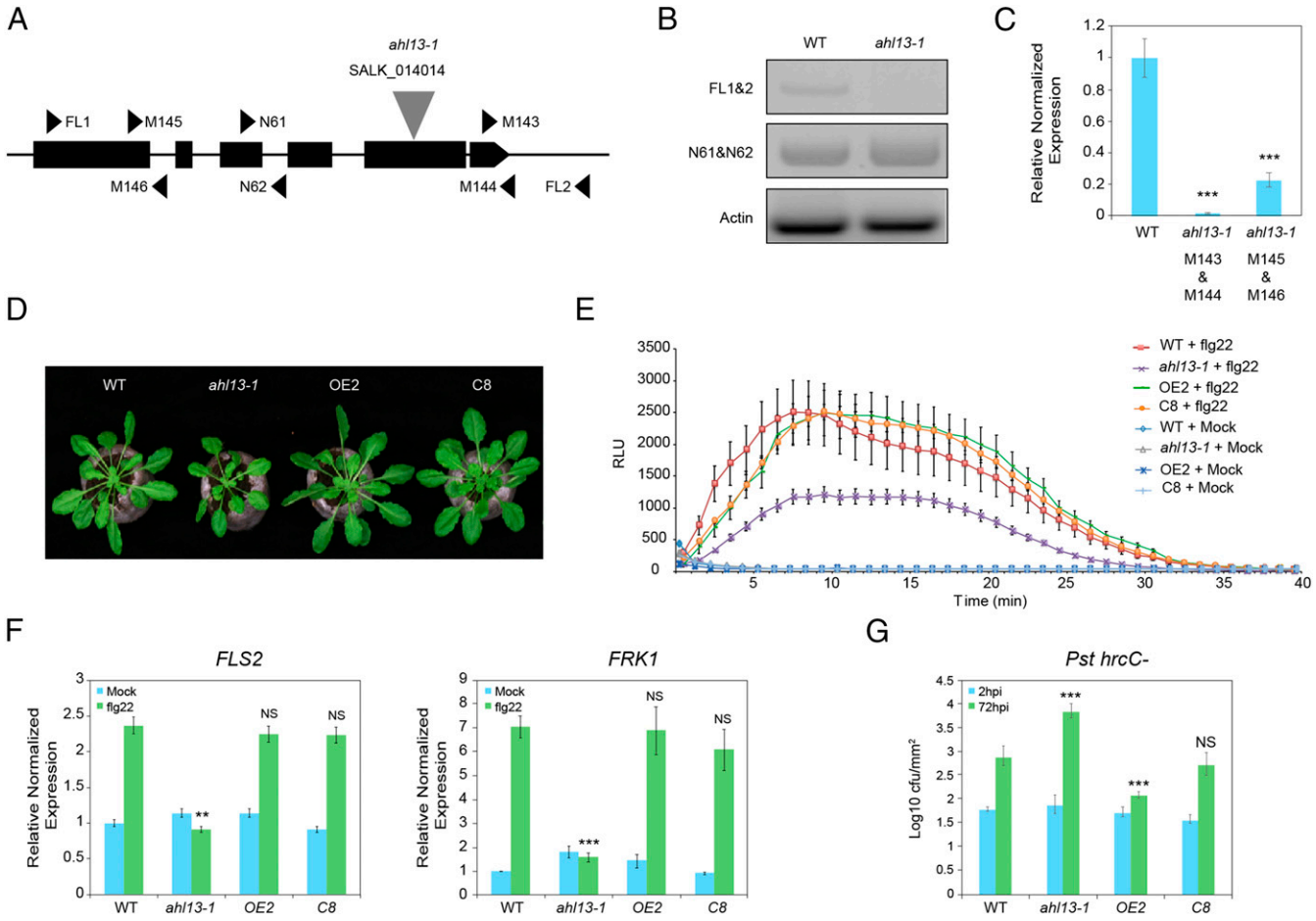


**Fig. 4.** Phenotyping of *ahl13-1* mutant plants. (*A*) Genomic organization and T-DNA insertion of *ahl13-1*. Exons are shown as solid black boxes. The site of T-DNA insertion is indicated by a gray inverted triangle. The arrowheads denote the position of the primers for RT-PCR and qRT-PCR. (*B*) RT-PCR of *ahl13-1* mutant. cDNA isolated from WT plants was used as a control. The amount of cDNA used as a template in RT-PCR reactions was normalized using the signal from the *ACTIN2* gene. (*C*) qRT-PCR of *ahl13-1* demonstrating that *AHL13* full-length transcript is not expressed in *ahl13-1* mutant. (*D*) Morphological phenotype of 4-wk-old WT, *ahl13-1* mutant, and OE2 and C8 transgenic plants. (*E*) Flg22-induced ROS burst in the WT, *ahl13-1,* OE2 and C8 plants. Leaf discs from 5-wk-old plants were treated with water or 1 μM flg22 over 40 min. (*F*) Flg22-induced *FLS2* and *FRK1* defense marker gene expression in *ahl13-1,* OE2 and C8 plants was determined by qRT-PCR relative to WT plants. (*G*) Four-week-old WT, *ahl13-1,* OE2, and C8 plants were spray inoculated with a *Pst hrcC*$^{-}$ bacterial suspension at an $OD_{600}$ = 0.002, and the bacterial titer was quantified at 2 and 72 h postinoculation. The data are shown as means from three biological replicates. Asterisks indicate significant differences compared to WT as determined by Mann–Whitney *U* test (***$P \leq 0.001$ and **$P \leq 0.01$). NS, not significant.

genes to WT levels was seen in OE2 and C8 lines (*SI Appendix*, Fig. S7). Due to the perturbation in several hormone-related genes, we quantified SA, JA, and JA-Ile levels. We observed a significant increase in JA and JA-Ile levels in *ahl13-1* compared with WT plants following infiltration with *Pst hrcC*$^{-}$, while JA and JA-Ile levels exhibited WT levels in the OE2 line (Fig. 5*E*). In contrast, we found that SA levels were not affected (Fig. 5*E*).

High JA levels are known to boost resistance to necrotrophic pathogens (64). Therefore, we challenged *ahl13-1* as well as the OE2 line to the necrotrophic fungal pathogen *Botrytis cinerea*. The *ahl13-1* mutant was more resistant to *B. cinerea*, while the OE2 line exhibited a WT-like response (Fig. 5*F*).

In the transcriptome analysis of *ahl13-1* upon *Pst hrcC*$^{-}$ infection, the JA biosynthesis gene *ALLENE OXIDE CYCLASE* (*AOC*) was found to be highly up-regulated. Therefore, we examined the expression levels of *AOC1*, *AOC2*, and *AOC3*. We found that all three genes showed significantly higher induction in *Pst hrcC*$^{-}$-infected *ahl13-1* plants when compared to WT (Fig. 5*G*). Furthermore, the expression levels of *AOC* genes were comparable to WT in the OE2 and C8 lines (Fig. 5*H* and *SI Appendix*, Fig. S8).

The *LIPOXYGENASE* (*LOX*) gene family members play a critical role in JA biosynthesis (65). The expression levels of *LOX2* and *LOX4* were altered in the transcriptome analysis, which prompted us to confirm their expression levels in *ahl13-1* mutant and transgenic lines. qRT-PCR analysis indicated that *Pst hrcC*$^{-}$ infection significantly increased the expression of *LOX2* and *LOX4* in *ahl13-1* when compared to WT (Fig. 5*G*) but not in the OE2 and C8 lines (Fig. 5*H* and *SI Appendix*, Fig. S8). These results confirm the transcriptome data and point to an important role for *AHL13* in defense response by modulating the expression of hormone-related genes.

The genes in cluster 1 of the heatmap (Fig. 5*A*) are highly induced in response to pathogen treatment. The GO enrichment in this cluster corresponds to response to JA, defense response, and glucosinolate metabolic process. It has been reported that the *Pst DC3000 hrcC*$^{-}$ polar strain that we used produces higher levels of coronatine (66). In order to determine the causal factor for the up-regulation of the genes in cluster 1, we treated WT as well as *ahl13-1* plants with the nonpolar *hrcC*$^{-}$ strain (*Pst DC3000 ΔhrcC::Km*$^{r}$-CUCPB5112) and verified the expression of eight genes from cluster 1. The genes we chose were *AOC1*, *AOC2*, *AOS*, *JAZ5*, *LOX2*, *VSP2*, *PDF1.2a*, and *PDF1.3*. We observed

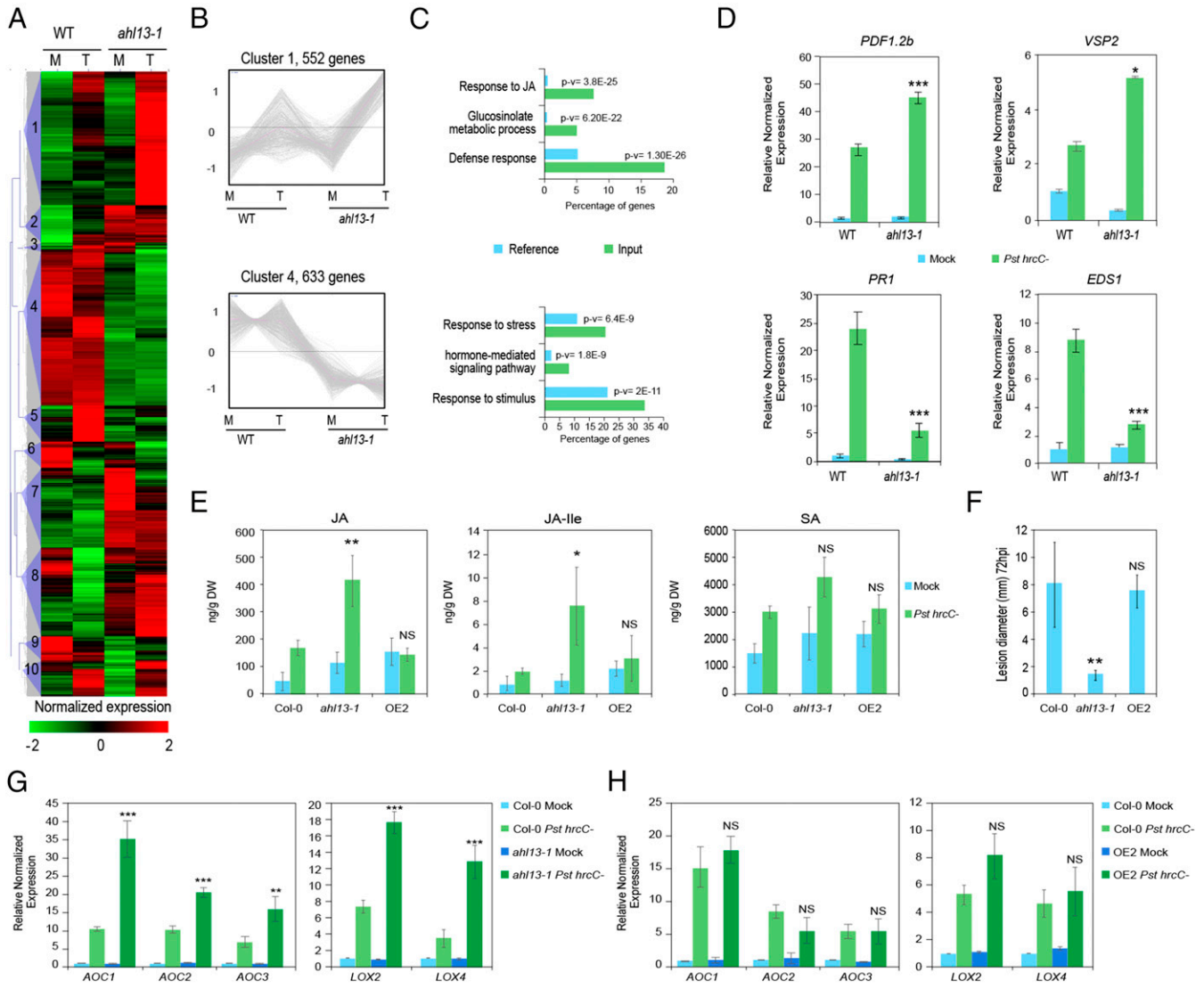


**Fig. 5.** Transcriptome profiling shows that *AHL13* regulates hormone and defense response genes. (*A*) Heatmap of mock and *Pst hrcC*$^{-}$-induced genes in WT and *ahl13-1* plants. The original fragments per kilobase per million values were subjected to data adjustment by normalized genes/rows and hierarchical clustering was generated with the average linkage method using MeV4.0. Red color indicates relatively high expression and green indicates relatively low expression. (*B*) Expression pattern of the gene clusters 1 and 4. (*C*) GO enrichment of genes for cluster 1 and cluster 4. The percent enrichment was calculated based on the frequency of genes annotated to the term compared with their frequency in the genome. (*D*) qRT-PCR analysis of *AHL13*-regulated genes in 14-d-old plants treated either with mock or *Pst hrcC*$^{-}$ for 24 h. (*E*) JA, JA-Ile, and SA levels in WT, *ahl13-1*, and OE2 plants were measured after infiltrated with *Pst hrcC*$^{-}$ ($OD_{600}$ = 0.2) at 0 and 1 d postinoculation. (*F*) The *ahl13-1* plants are insensitive to *B. cinerea* infection. Four-week-old WT, *ahl13-1,* and OE2 plants were drop-inoculated with *B. cinerea* spore suspension at a density of $5 \times 10^6$ spores per milliliter. The inoculated leaves from three different plants were harvested and pictures were taken for lesion measurements. Lesion diameter was measured using ImageJ analysis tool. (*G*) qRT-PCR analysis of *AOC1*, *AOC2*, *AOC3*, *LOX2*, and *LOX4* genes in WT and *ahl13-1* plants with and without *Pst hrcC*$^{-}$ treatment. (*H*) qRT-PCR analysis of *AOC1*, *AOC2*, *AOC3*, *LOX2*, and *LOX4* genes in WT and OE2 plants with and without *Pst hrcC*$^{-}$ treatment. Asterisks indicate significant differences compared to WT as determined by Mann–Whitney *U* test (***$P \leq 0.001$, **$P \leq 0.01$, and *$P \leq 0.05$). NS, not significant.

that the expression pattern of all of the selected genes was similar to what we had observed earlier; that is, they are induced to a much higher degree in the *ahl13-1*–treated plants (*SI Appendix*, Fig. S9*A*). We also carried out bacterial infection studies on the WT, *ahl13-1*, OE2, and C8 lines with the nonpolar *hrcC*$^{-}$ strain CUCPB5112 and observed that the plants behaved similar to when they were treated with the polar *hrcC*$^{-}$ strain, further indicating that the observed effects are not due to the higher levels of coronatine in the polar *hrcC*$^{-}$ strain (*SI Appendix*, Fig. S9*B*).

**Phosphorylation Stabilizes AHL13.** To determine the biological function of the identified S109 and S376 phosphorylation sites, we generated the following *AHL13* constructs for expression in planta: WT (*Pro35S::AHL13*$^{wt}$*-GFP*), phospho-dead (*ProUbi::AHL13*$^{S109A/S376A}$*-GFP*), and phospho-mimic (*ProUbi::AHL13*$^{S109D/S376D}$*-GFP*) by site-directed mutagenesis. We then examined the subcellular localization of these GFP-tagged proteins expressed transiently in *N. benthamiana* leaf epidermal cells by confocal microscopy. Both $AHL13^{wt}$ and $AHL13^{S109D/S376D}$ proteins were localized to the nucleus; however, we were unable to detect $AHL13^{S109A/S376A}$ (Fig. 6*A*). These observations suggested that phosphorylation of AHL13 might play a role in AHL13 protein accumulation or subcellular localization.

To further examine these hypotheses, we generated stable lines in the *ahl13-1* mutant background: OE2 overexpression and C8 complementation (*ahl13-1 Pro35S::AHL13*$^{wt}$*-GFP*), AA2

phospho-dead (*ahl13-1 ProUbi::AHL13*$^{S109A/S376A}$*-GFP*), and DD1 phospho-mimic (*ahl13-1 ProUbi::AHL13*$^{S109D/S376D}$*-GFP*). Examination of AHL13-GFP localization in the roots of these transgenic plants revealed nuclear localization for AHL13-GFP in the OE2, C8, DD1, and AA2 transgenic lines, but in the case of AA2 lines the GFP signal was very weak (Fig. 6*B*). This finding further pointed toward an effect of the two phosphosites on AHL13 protein accumulation, but not to its subcellular localization. Importantly, there is no obvious difference observed for *AHL13* transcript levels between the C8, DD1, and AA2 lines (*SI Appendix*, Fig. S4), suggesting that the reduced AHL13 protein accumulation in the AA2 line is modulated at the protein level.

To confirm this hypothesis, we examined the stability of AHL13 in WT, OE2, C8, DD1, and AA2 lines. To determine whether the ubiquitin-proteasome pathway is involved in the degradation of AHL13, 10-d-old seedlings were treated with or without the proteasomal inhibitor MG132 for 2 h. Then total proteins were extracted and AHL13-GFP was analyzed by immunoblotting using an anti-GFP antibody. As shown in Fig. 6*C* and *SI Appendix*, Fig. S10, without MG132 treatment and using the WT nontagged line as negative control, the GFP-tagged AHL13 was detected in all lines except for the AA2 line. In contrast, upon MG132 treatment, AHL13-GFP protein was also detected in the AA2 line, indicating that AHL13$^{S109A/S376A}$ is degraded by the proteasome-dependent pathway. We next examined the levels of GFP-tagged AHL13 in the roots of the AA2 and DD1 plants following treatment with and without MG132. We observed normal nuclear localization for AHL13 in the DD1 line but only a very weak fluorescent signal of the GFP-tagged AHL13 in the AA2 line (Fig. 6*D*). However, the GFP-tagged AHL13 fluorescence in the AA2 roots could be enhanced following a 2-h treatment with MG132. AA2 and DD1 lines did not display phenotypic changes with respect to morphology or pathogen infection, suggesting that the two phosphorylation sites do not have a role in development (Fig. 6*E*). To see an effect of the AA and DD mutations on pathogenesis, we challenged the plants with *Pst hrcC*$^{-}$. While the DD1 line showed WT-like behavior, the AA2 line behaved like the *ahl13-1* mutant plants, further reinforcing the fact that in the AA2 line the protein is degraded and the plants become more susceptible to the pathogen (Fig. 6*F*).

The structural information of a protein provides valuable information about its function, stability, and other properties. Therefore, we performed protein structure homology modeling of AHL13. AHL13 contains a PPC domain (residues 222 to 344) flanked by large flexible regions (221 residues upstream and 95 residues downstream) (Fig. 6*G*). The N-terminal flexible segment contains two AT-hook domains (residues 131 to 143 and 196 to 208) and has a very basic calculated pI of 9.99, supporting DNA interactions. The phosphorylated serine residues S109 and S376 of AHL13 are located within the unstructured segments that are freely accessible to interaction with other proteins, such as the MAPKs for phosphorylation. The three-dimensional structure of the PPC domain can be modeled based on 20 to 23% identical regions from known PPC domains. PPC domains consistently form homotrimers, and the preservation of the hydrophobic interface between the monomers strongly supports that this is also the case for AHL13. Our results demonstrated that unphosphorylated AHL13 is subject to rapid proteasomal degradation. Given their location in the flexible regions, phosphorylation of S109/S376 cannot directly stabilize the PPC domain. However, it is possible that the negatively charged phosphate groups stabilize the relatively prominent basic surface patches of AHL13 (Fig. 6*H*), which could enhance protein stability. Such phosphate interactions are supported by sulfate ions identified on similar surface patches identified on the PPC domain from the *Bacteroides thetaiotaomicron* vpi-5482 protein bt_1116 (PDB ID code 3HTN). An alternative, but possibly synergistic mechanism would be that serine phosphorylation leads to charge–charge interactions (within the flexible regions or with the PPC core) that conceal proteasomal targeting signals, such as ubiquitination sites.

Overall, these observations suggest that the AHL13$^{S109/S376}$ phosphosites play an important role in AHL13 protein stability.

## Discussion

Although a number of potential substrates have been identified, the role of MPK3, MPK4, and MPK6 in regulating chromatin organization and epigenetic events has been poorly studied. In this work, we used a quantitative phosphoproteomic approach to identify putative chromatin targets. Among 46 proteins, whose phosphorylation status changes upon flg22 treatment or in a particular *MAPK* mutant, we identified a number of factors involved in chromatin organization, components involved in DNA-binding or RNA polymerase complex function, and last but not least several factors involved in splicing and RNA processing.

**Transcription Factors and Repressors.** A number of transcription factors with a known role in immunity were identified. We recently characterized the Trihelix Transcription factor GT2-like 1 (GTL1) as part of the MPK4 pathway that acts as a positive regulator of bacterial-triggered immunity and SA homeostasis (67). Another interesting factor is TIC, which plays a role in the circadian rhythm and in JA signaling by interacting with the transcription factor MYC2 (68). Transcriptional repression is equally important in regulating gene expression and corepressors, such as TPL play an important role in multiple hormonal signaling cascades (69). Our chromatin phosphoproteome revealed that TPL is de novo-phosphorylated in response to flg22 in the *mpk3* mutant. Interestingly, TPL does not directly interact with DNA, but interacts with a variety of sequence-specific transcription factors, recruiting chromatin remodeling factors to down-regulate genes (70).

**Chromatin Organization and Regulation.** Several factors regulating the immune receptor SNC1 (SUPPRESSOR OF npr1-1, CONSTITUTIVE1) were identified as MAPK targets, including CHR5 and MOS1. Both CHR5 and MOS1 function antagonistically with DDM1 (DECREASED DNA METHYLATION 1) by regulating nucleosome occupancy and DNA methylation levels in the promoter region of *SNC1* (71, 72). These results suggest that MAPK signaling might regulate accessibility of the *SNC1* gene locus and thereby its expression levels.

A chromatin factor that plays a role in reading histone modifications is the PH domain containing protein EARLY BOLTING IN SHORT DAYS (EBS) functioning in floral initiation (73). EBS recognizes di- and trimethylated H3K4 to maintain an inactive chromatin conformation of its target genes *SOC1* and *FT*. EBS is widely conserved in plants but absent in other eukaryotes, suggesting that the regulatory module mediated by these proteins could represent a distinct mechanism for gene expression control in plants.

**RNA Processing.** Multiple putative MAPK targets were identified as proteins with a role in RNA processing. But, no functional data are so far available for most of these proteins. One exception is nucleolin, which is a major nucleolar protein implicated in many aspects of ribosomal biogenesis, including processing of the 35S preribosomal RNA. Nucleolin was also found to regulate DNA methylation and expression of the *rRNA* gene locus in *Arabidopsis* (73). It will be interesting to study the role of phosphorylation in nucleolin functioning during immunity.

**Regulation of PAMP-Induced AHL Phosphorylation by MAPKs.** In this work, we identified two members of the *AHL* gene family as potential targets of MAPK signaling, AHL13 and AHL10 (AT2G33620), which are closely related clade B homologs (43). Recent studies identified AHL13 and AHL10 to be phosphoproteins (34, 61–63, 75). Notably, a study, using dexamethasone

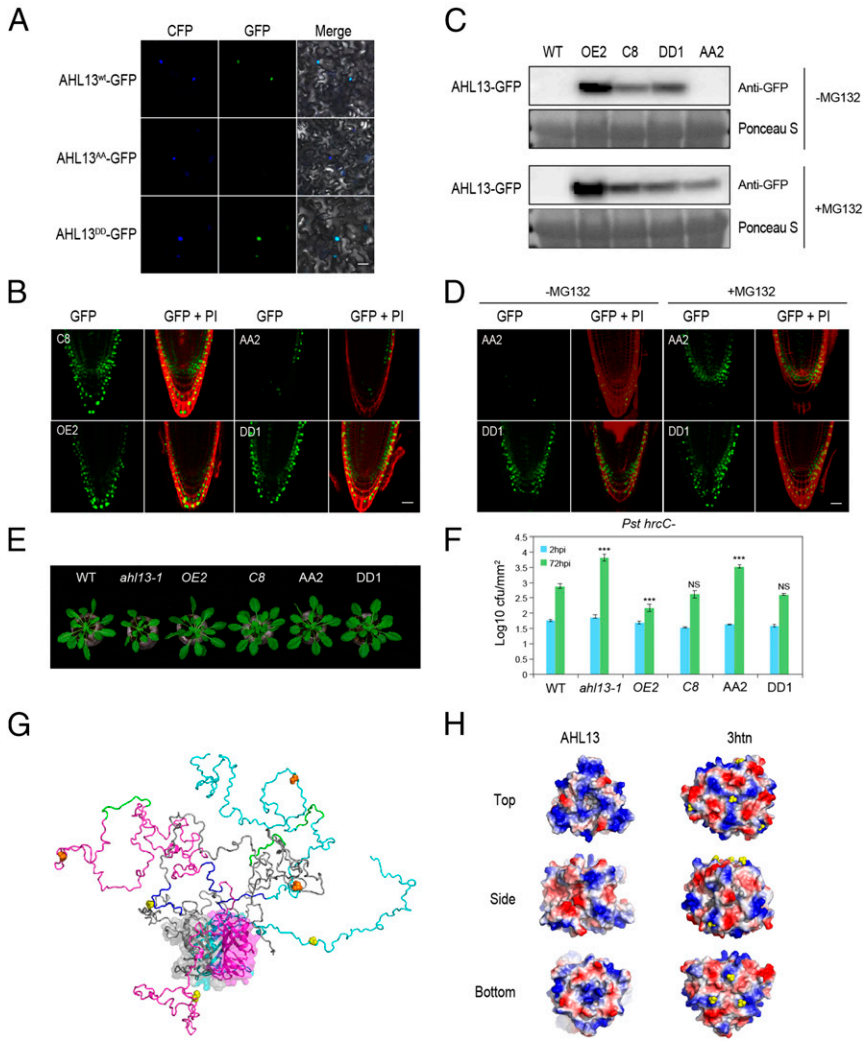


**Fig. 6.** AHL13$^{S109/S376}$ phosphosites affect AHL13 protein stability. (*A*) Subcellular localization of transiently expressed *pro35S:AHL13$^{wt}$-GFP*, *proUbi:AHL13$^{S109A/S376A}$-GFP*, *proUbi:AHL13$^{S109D/S376D}$-GFP*, and *proUbi:Serrate-CFP* in *N. benthamiana* leaves. *proUbi:Serrate-CFP* served as the control nuclear marker. The localization was visualized 48 h after infiltration by laser scanning confocal microscopy. GFP fluorescence is in green and CFP fluorescence is in blue. (Scale bar, 20 μm.) (*B*) AHL13-GFP expression and protein localization in *Arabidopsis* root tips of 8-d-old *ahl13-1 pro35S:AHL13$^{wt}$-GFP* (C8), *ahl13-1 pro35S:AHL13$^{wt}$-GFP* (OE2), phospho-dead *ahl13-1 proUbi:AHL13$^{S109A/S376A}$-GFP* (AA2), and phospho-mimic *ahl13-1 proUbi:AHL13$^{S109D/S376D}$-GFP* (DD1). (Scale bar, 20 μm.) (*C*) Immunoblotting of AHL13-GFP in WT, OE2, C8, DD1, and AA2 stable lines. Total protein was extracted from 10-d-old seedlings after treating with and without 50 μM MG132 for 2 h. AHL13-GFP was analyzed by immunoblotting using anti-GFP antibody and the proteins were stained with Ponceau-S for loading control. (*D*) AHL13-GFP expression and protein localization in *Arabidopsis* root tips of 8-d-old AA2 and DD1 with and without 50 μM MG132 treatment. Confocal laser scanning microscopy images of GFP fluorescence (green) and propidium iodide (PI) fluorescence (red) of *Arabidopsis* roots. (Scale bar, 20 μm.) (*E*) Morphological phenotype of 4-wk-old WT, *ahl13-1* mutant, OE2, C8, AA2, and DD1 plants. This photograph is an extension of the photograph of plants shown in Fig. 4*D*. (*F*) Four-week-old WT, *ahl13-1*, OE2 C8, AA2, and DD1 plants were spray-inoculated with a *Pst hrcC*$^{-}$ bacterial suspension at an $OD_{600}$ = 0.002, and the bacterial titer was quantified at 2 and 72 h postinoculation. The data are shown as means from three biological replicates. Asterisks indicate significant differences compared to WT as determined by Mann–Whitney *U* test (***$P \leq 0.001$). NS, not significant. (*G*) Theoretical model of the AHL13 trimer. The three protein chains are colored gray, cyan and magenta. The secondary structure and semitransparent surface of the PPC domains are shown. The N- and C-terminal extensions are modeled in stereochemically plausible random orientations. The AT hook domains are shown in green and blue. S109 and S376 are shown as orange and yellow spheres, respectively. (*H*) Electrostatic surface of the PPC domain, color-ramped from red: acidic, to blue: basic. Top, side, and bottom views with respect to *A* are shown for AHL13 (homology model) and for the *B. thetaiotaomicron* vpi-5482 protein bt_1116 (PDB ID code 3HTN). Sulfate ions present in the crystal structure of bt_1116 are shown as yellow spheres to illustrate the possibility of associations of phosphate groups with the AHL13 PPC domain.

inducible NtMEK2 activation, suggested that AHL13 might be targeted by MPK3 and MPK6 in vivo, and AHL13 S376 phosphorylation was reported to be induced in vivo after a 30-min flg22 treatment (34, 62). This prompted us to investigate the role of AHL13 in plant immunity. Here, we show that AHL13 preferentially interacts with MPK6 in vivo but can be phosphorylated in vitro by MPK3, MPK4, and MPK6. Transcriptome analysis of *ahl13* mutants and WT showed that AHL13 regulates the expression of JA biosynthesis and signaling genes. Interestingly, AHLs from *Catharanthus roseus* have been shown to bind to and regulate the jasmonate-response element of the JA-regulated ORCA3 transcription factor (76). Enhanced JA levels in *ahl13* mutant plants also correlated with the increased and decreased resistance phenotypes to necrotrophic *B. cinerea* and hemibiotrophic *P. syringae* strains, respectively, in agreement with the known role of JA in the defense against these different pathogens (64). We looked for enrichment of motifs in the promoters of the genes that were found to be deregulated in the transcriptome of *ahl13* (*SI Appendix*, Fig. S11). While no interesting motifs were enriched in the promoters of the up-regulated genes, the motif with highest enrichment in the promoters of the down-regulated genes was KUA1 or KUODAI1, which is an MYB transcription factor that regulates ROS homeostasis and cell elongation (77). Although KUA1 has not been shown to be involved in immunity, its role in ROS homeostasis fits well to the function of AHL13. Moreover, *ahl13* plants have reduced size, like *kua1*.

Another interesting motif that was found to be enriched was TGA2, a key factor in SA signaling that interacts with NPR1 (78). This further reinforces the role of AHL13 in hormone biosynthesis and signaling. Finally, along with bZIP16, another motif was that of VIP1, another bZIP transcription factor that is a direct target of MPK3 to regulate several flg22-induced genes (79, 80). We also showed that MAPK phosphorylation of S109 and S376 is essential for protein stability of AHL13. MPK3, MPK4, and MPK6, as well as AHL13, are expressed in virtually all plant tissues (63) (*SI Appendix*, Fig. S12). Interestingly, phosphorylation of AHL13 at S109 and S376 is found in all or most tissues (63), strongly suggesting that regulation of AHL13 stability by MAPKs is a ubiquitous mechanism for plant defense (Dataset S7). Our phosphoproteomic analysis also indicated that S314 phosphorylation of AHL10 was dependent on *MPK6* (*SI Appendix*, Fig. S13 and Dataset S2). Interestingly, AHL13 S376 corresponds to AHL10 S314, whose dephosphorylation was shown to be critical for growth regulation under low-water potential stress (56). It is thus tempting to

speculate that MPK6 could be involved in AHL10 S314 phosphorylation to regulate growth during water stress.

## Conclusions

The phosphoproteomic analysis of chromatin in response to flagellin treatment revealed a number of novel proteins to be targeted by PAMP-induced signaling. Moreover, our analysis of *mpk3*, *mpk4*, and *mpk6* provided evidence that MAPK signaling is not only linked to RNA transcription and processing, but also to the regulation of chromatin organization. In agreement with previous studies, we could confirm that the three MAPKs have both specific and shared substrates, which may explain a number of discrepancies in the literature on the roles and specificities of some of these substrates in MAPK signaling. Overall, the identification of a panel of phosphorylated chromatin targets provides the basis for future functional studies on the role of chromatin organization, regulation of transcription, and RNA processing in immunity.

## Experimental Procedures

**Plant Material and Culture Conditions.** For phosphoproteomic analyses, *Arabidopsis thaliana* ecotype Columbia-0 (Col-0) was used as WT plant. The three *mapk* knockout mutants were *mpk3-1* (SALK_151594) (81), *mpk4-2* (SALK_056245) (17), and *mpk6-2* (SALK_073907) (81), which were generated in the Col-0 genetic background. The T-DNA insertion mutant used for *ahl13-1* was SALK_014014. T-DNA insertion was confirmed by PCR using a primer specific to the T-DNA border (LBb1.3 primer for SALK lines: 5′-ATTTTGCCGATTTCGGAAC-3′) and gene-specific primers for the T-DNA insertion line. Primer sequences are provided in Dataset S8. Plant growth, treatment, and harvest were done as described previously in Rayapuram et al. (37).

*N. benthamiana* plants were grown in the greenhouse at 28 °C under 70% humidity and 16-h/8-h light conditions. Four-week-old plants were used for transient leaf transformation by agroinfiltration to carry out BiFC and subcellular localization assays.

**Isolation of Chromatin-Associated Proteins and Phosphopeptide Enrichment.** Nuclear and chromatin-associated proteins were isolated exactly as described previously in Bigeard et al. (82). The detailed methodology is described in *SI Appendix*.

**LC-MS/MS Analyses of Phosphopeptide Samples and of Nonmodified Peptides.** The experimental details and the relevant methods for LC-MS/MS analyses are described in *SI Appendix*.

**Bioinformatic Analyses.** The lists of phosphopeptides identified with precise phosphosites were submitted to the program motif-x (58) to identify enriched phosphorylation motifs. String networks were generated using the STRING: Functional protein association networks (v10.5) tool (60) within the Cytoscape environment (83). AgriGO (agriGO v2.0) was used for all GO analyses (84). The enrichment of GO terms in relation to total nuclear proteome was also searched with AgriGO, using as customized reference the genes predicted by SUBAcon predictor to code for proteins with nuclear localization and the genes for which there is an experimental evidence that the corresponding proteins are located in the nucleus (85, 86). Putative MAPK docking sites were searched using the ELM program (http://elm.eu.org/) (87) with the UniProtKB identifier of the proteins of interest.

**Gene Cloning and Protein Methods.** All the methods related to gene cloning, recombinant protein expression and purification, phosphorylation assay, BiFC, GST pull-down assay, and subcellular localization are described in *SI Appendix*.

**PAMP-Induced Oxidative Burst.** PAMP-induced oxidative burst was carried out as described previously (88).

***P. syringae* and *B. cinerea* Infection Studies.** The procedures for carrying out pathogen infection studies are described in detail in *SI Appendix*.

**RNA Extraction, qRT-PCR, and Transcriptome Analysis.** The methods pertaining to RNA extraction, qRT-PCR, and transcriptome analysis are presented in *SI Appendix*.

**Phytohormone Measurements.** Phytohormones were quantified essentially as described previously (89).

**Protein Structure Homology Modeling.** Trimeric models for AHL13 were produced with SWISS-MODEL (90) based on the available 20 to 23% identical PPC crystal structures PDB ID codes 2DT4, 2HX0, 2NMU, 3HTN (QMEAN scores were between −1.7 and −2.1), and analyzed with pymol (http://pymol.org). The complete AHL13 model shown in Fig. 6*G* was built using 2DT4 as template for the PPC domain. The N- and C-terminal extensions are modeled using our in-house program MULTIPROT.

**Data Availability.** The MS proteomics data have been deposited to the ProteomeXchange Consortium via PRIDE (91) partner repository (dataset identifier PXD009823 and DOI: 10.6019/PXD009823). The RNA-seq data have been deposited in the National Center for Biotechnology Information's Gene Expression Omnibus database, https://www.ncbi.nlm.nih.gov/geo (accession no. GSE119465).

**ACKNOWLEDGMENTS.** We thank Véronique Legros, Huma Khurram, and Huoming Zhang for technical assistance in mass spectometry; Stéphanie Pateyron and Alexandra Avon for technical support in molecular biology; and Jean Colcombet for kindly providing the constitutively active MAPK vectors. This work was supported by Agence Nationale de la Recherche ANR-2010-JCJC-1608 and ANR-14-CE19-0014 (to D.P.); Investissement d'Avenir Infrastructures Nationales en Biologie et Santé program (ProFI project, ANR-10-INBS-08); and by King Abdullah University of Science and Technology BAS/1/1062-01-01 (to H.H.). The Institute of Plant Sciences Paris-Saclay benefits from the support of the LabEx Saclay Plant Sciences (ANR-10-LABX-0040-SPS). M.A.-T. was supported by a Humboldt-Capes fellowship.

1. A. M. Klein, E. Zaganjor, M. H. Cobb, Chromatin-tethered MAPKs. *Curr. Opin. Cell Biol.* **25**, 272–277 (2013).
2. E. de Nadal, F. Posas, Multilayered control of gene expression by stress-activated protein kinases. *EMBO J.* **29**, 4–13 (2010).
3. J. Bigeard, H. Hirt, Nuclear signaling of plant MAPKs. *Front. Plant Sci.* **9**, 469 (2018).
4. D. K. Pokholok, J. Zeitlinger, N. M. Hannett, D. B. Reynolds, R. A. Young, Activated signal transduction kinases frequently occupy target genes. *Science* **313**, 533–536 (2006).
5. S. Healy, P. Khan, S. He, J. R. Davie, Histone H3 phosphorylation, immediate-early gene expression, and the nucleosomal response: A historical perspective. *Biochem. Cell Biol.* **90**, 39–54 (2012).
6. J. I. Wu, J. Lessard, G. R. Crabtree, Understanding the words of chromatin regulation. *Cell* **136**, 200–206 (2009).
7. G. Mas *et al.*, Recruitment of a chromatin remodelling complex by the Hog1 MAP kinase to stress genes. *EMBO J.* **28**, 326–336 (2009).
8. M. Proft *et al.*, The stress-activated Hog1 kinase is a selective transcriptional elongation factor for genes responding to osmotic stress. *Mol. Cell* **23**, 241–250 (2006).
9. T. Suganuma *et al.*, The ATAC acetyltransferase complex coordinates MAP kinases to regulate JNK target genes. *Cell* **142**, 726–736 (2010).
10. G. Komis, O. Šamajová, M. Ovečka, J. Šamaj, Cell and developmental biology of plant mitogen-activated protein kinases. *Annu. Rev. Plant Biol.* **69**, 237–265 (2018).
11. X. Meng, S. Zhang, MAPK cascades in plant disease resistance signaling. *Annu. Rev. Phytopathol.* **51**, 245–266 (2013).
12. M. C. Rodriguez, M. Petersen, J. Mundy, Mitogen-activated protein kinase signaling in plants. *Annu. Rev. Plant Biol.* **61**, 621–649 (2010).
13. H. Li *et al.*, MPK3- and MPK6-mediated ICE1 phosphorylation negatively regulates ICE1 stability and freezing tolerance in Arabidopsis. *Dev. Cell* **43**, 630–642.e4 (2017).
14. M. Teige *et al.*, The MKK2 pathway mediates cold and salt stress signaling in Arabidopsis. *Mol. Cell* **15**, 141–152 (2004).
15. C. Zhao *et al.*, MAP kinase cascades regulate the cold response by modulating ICE1 protein stability. *Dev. Cell* **43**, 618–629.e5 (2017).
16. M. Beck, G. Komis, J. Müller, D. Menzel, J. Samaj, Arabidopsis homologs of nucleus- and phragmoplast-localized kinase 2 and 3 and mitogen-activated protein kinase 4 are essential for microtubule organization. *Plant Cell* **22**, 755–771 (2010).
17. K. Kosetsu *et al.*, The MAP kinase MPK4 is required for cytokinesis in Arabidopsis thaliana. *Plant Cell* **22**, 3778–3790 (2010).
18. Q. Zeng, J. G. Chen, B. E. Ellis, AtMPK4 is required for male-specific meiotic cytokinesis in Arabidopsis. *Plant J.* **67**, 895–906 (2011).
19. W. Jia *et al.*, Mitogen-activated protein kinase cascade MKK7-MPK6 plays important roles in plant development and regulates shoot branching by phosphorylating PIN1 in Arabidopsis. *PLoS Biol.* **14**, e1002550 (2016).
20. H. Wang, N. Ngwenyama, Y. Liu, J. C. Walker, S. Zhang, Stomatal development and patterning are regulated by environmentally responsive mitogen-activated protein kinases in Arabidopsis. *Plant Cell* **19**, 63–73 (2007).
21. Y. Zhang, P. Wang, W. Shao, J. K. Zhu, J. Dong, The BASL polarity protein controls a MAPK signaling feedback loop in asymmetric cell division. *Dev. Cell* **33**, 136–149 (2015).
22. J. Bigeard, J. Colcombet, H. Hirt, Signaling mechanisms in pattern-triggered immunity (PTI). *Mol. Plant* **8**, 521–539 (2015).
23. H. Cui, K. Tsuda, J. E. Parker, Effector-triggered immunity: From pathogen perception to robust defense. *Annu. Rev. Plant Biol.* **66**, 487–511 (2015).

24. R. Hückelhoven, Cell wall-associated mechanisms of disease resistance and susceptibility. *Annu. Rev. Phytopathol.* **45**, 101–127 (2007).
25. I. Ahuja, R. Kissen, A. M. Bones, Phytoalexins in defense against pathogens. *Trends Plant Sci.* **17**, 73–90 (2012).
26. L. C. van Loon, M. Rep, C. M. Pieterse, Significance of inducible defense-related proteins in infected plants. *Annu. Rev. Phytopathol.* **44**, 135–162 (2006).
27. L. Gómez-Gómez, T. Boller, FLS2: An LRR receptor-like kinase involved in the perception of the bacterial elicitor flagellin in Arabidopsis. *Mol. Cell* **5**, 1003–1011 (2000).
28. G. Bethke *et al*., Activation of the Arabidopsis thaliana mitogen-activated protein kinase MPK11 by the flagellin-derived elicitor peptide, flg22. *Mol. Plant Microbe Interact.* **25**, 471–480 (2012).
29. N. Frei dit Frey *et al*., Functional analysis of Arabidopsis immune-related MAPKs uncovers a role for MPK3 as negative regulator of inducible defences. *Genome Biol.* **15**, R87 (2014).
30. Y. Nitta, P. Ding, Y. Zhang, Identification of additional MAP kinases activated upon PAMP treatment. *Plant Signal. Behav.* **9**, e976155 (2014).
31. G. Bi *et al*., Receptor-like cytoplasmic kinases directly link diverse pattern recognition receptors to the activation of mitogen-activated protein kinase cascades in Arabidopsis. *Plant Cell* **30**, 1543–1561 (2018).
32. M. Gao *et al*., MEKK1, MKK1/MKK2 and MPK4 function together in a mitogen-activated protein kinase cascade to regulate innate immunity in plants. *Cell Res.* **18**, 1190–1198 (2008).
33. J. L. Qiu *et al*., Arabidopsis mitogen-activated protein kinase kinases MKK1 and MKK2 have overlapping functions in defense signaling mediated by MEKK1, MPK4, and MKS1. *Plant Physiol.* **148**, 212–222 (2008).
34. W. Hoehenwarter *et al*., Identification of novel in vivo MAP kinase substrates in Arabidopsis thaliana through use of tandem metal oxide affinity chromatography. *Mol. Cell. Proteomics* **12**, 369–380 (2013).
35. N. V. Huck *et al*., Combined $^{15}$N-labeling and TandemMOAC quantifies phosphorylation of MAP kinase substrates downstream of MKK7 in *Arabidopsis*. *Front. Plant Sci.* **8**, 2050 (2017).
36. I. Lassowskat, C. Böttcher, L. Eschen-Lippold, D. Scheel, J. Lee, Sustained mitogen-activated protein kinase activation reprograms defense metabolism and phosphoprotein profile in Arabidopsis thaliana. *Front. Plant Sci.* **5**, 554 (2014).
37. N. Rayapuram *et al*., Quantitative phosphoproteomic analysis reveals shared and specific targets of *Arabidopsis* mitogen-activated protein kinases (MAPKs) MPK3, MPK4, and MPK6. *Mol. Cell. Proteomics* **17**, 61–80 (2018).
38. Arabidopsis Genome Initiative, Analysis of the genome sequence of the flowering plant Arabidopsis thaliana. *Nature* **408**, 796–815 (2000).
39. A. H. Paterson *et al*., The Sorghum bicolor genome and the diversification of grasses. *Nature* **457**, 551–556 (2009).
40. S. A. Rensing *et al*., The Physcomitrella genome reveals evolutionary insights into the conquest of land by plants. *Science* **319**, 64–69 (2008).
41. G. A. Tuskan *et al*., The genome of black cottonwood, Populus trichocarpa (Torr. & Gray). *Science* **313**, 1596–1604 (2006).
42. J. Yu *et al*., A draft sequence of the rice genome (Oryza sativa L. ssp. indica). *Science* **296**, 79–92 (2002).
43. J. Zhao, D. S. Favero, H. Peng, M. M. Neff, Arabidopsis thaliana AHL family modulates hypocotyl growth redundantly by interacting with each other via the PPC/DUF296 domain. *Proc. Natl. Acad. Sci. U.S.A.* **110**, E4688–E4697 (2013).
44. K. H. Ng, H. Yu, T. Ito, AGAMOUS controls GIANT KILLER, a multifunctional chromatin modifier in reproductive organ patterning and differentiation. *PLoS Biol.* **7**, e1000251 (2009).
45. I. H. Street, P. K. Shah, A. M. Smith, N. Avery, M. M. Neff, The AT-hook-containing proteins SOB3/AHL29 and ESC/AHL27 are negative modulators of hypocotyl growth in Arabidopsis. *Plant J.* **54**, 1–14 (2008).
46. C. Xiao, F. Chen, X. Yu, C. Lin, Y. F. Fu, Over-expression of an AT-hook gene, AHL22, delays flowering and inhibits the elongation of the hypocotyl in Arabidopsis thaliana. *Plant Mol. Biol.* **71**, 39–50 (2009).
47. J. Yun, Y. S. Kim, J. H. Jung, P. J. Seo, C. M. Park, The AT-hook motif-containing protein AHL22 regulates flowering initiation by modifying FLOWERING LOCUS T chromatin in Arabidopsis. *J. Biol. Chem.* **287**, 15307–15316 (2012).
48. J. Zhou, X. Wang, J. Y. Lee, J. Y. Lee, Cell-to-cell movement of two interacting AT-hook factors in Arabidopsis root vascular tissue patterning. *Plant Cell* **25**, 187–201 (2013).
49. O. Karami *et al*., A suppressor of axillary meristem maturation promotes longevity in flowering plants. *Nat. Plants* **6**, 368–376 (2020).
50. M. Širl *et al*., At-hook motif nuclear localised protein 18 as a novel modulator of root system Architecture. *Int. J. Mol. Sci.* **21**, E1886 (2020).
51. D. S. Favero *et al*., AT-hook transcription factors restrict petiole growth by antagonizing PIFs. *Curr. Biol.* **30**, 1454–1466.e6 (2020).
52. A. Matsushita, T. Furumoto, S. Ishida, Y. Takahashi, AGF1, an AT-hook protein, is necessary for the negative feedback of AtGA3ox1 encoding GA 3-oxidase. *Plant Physiol.* **143**, 1152–1162 (2007).
53. K. Lee, P. J. Seo, Coordination of matrix attachment and ATP-dependent chromatin remodeling regulate auxin biosynthesis and Arabidopsis hypocotyl elongation. *PLoS One* **12**, e0181804 (2017).
54. K. A. Yadeta *et al*., The Arabidopsis thaliana DNA-binding protein AHL19 mediates verticillium wilt resistance. *Mol. Plant Microbe Interact.* **24**, 1582–1591 (2011).
55. H. Lu, Y. Zou, N. Feng, Overexpression of AHL20 negatively regulates defenses in Arabidopsis. *J. Integr. Plant Biol.* **52**, 801–808 (2010).
56. M. M. Wong *et al*., Phosphoproteomics of *Arabidopsis* Highly ABA-induced1 identifies AT-Hook-Like10 phosphorylation required for stress growth regulation. *Proc. Natl. Acad. Sci. U.S.A.* **116**, 2354–2363 (2019).
57. S. Fujimoto *et al*., Identification of a novel plant MAR DNA binding protein localized on chromosomal surfaces. *Plant Mol. Biol.* **56**, 225–239 (2004).
58. M. F. Chou, D. Schwartz, Biological sequence motif discovery using motif-x. *Curr. Protoc. Bioinformatics*, 10.1002/0471250953.bi1315s35 (2011).
59. MAPK Group, Mitogen-activated protein kinase cascades in plants: A new nomenclature. *Trends Plant Sci.* **7**, 301–308 (2002).
60. A. Franceschini *et al*., STRING v9.1: Protein-protein interaction networks, with increased coverage and integration. *Nucleic Acids Res.* **41**, D808–D815 (2013).
61. E. Roitinger *et al*., Quantitative phosphoproteomics of the ataxia telangiectasia-mutated (ATM) and ataxia telangiectasia-mutated and rad3-related (ATR) dependent DNA damage response in Arabidopsis thaliana. *Mol. Cell. Proteomics* **14**, 556–571 (2015).
62. P. Wang *et al*., Mapping proteome-wide targets of protein kinases in plant stress responses. *Proc. Natl. Acad. Sci. U.S.A.* **117**, 3270–3280 (2020).
63. J. Mergner *et al*., Mass-spectrometry-based draft of the Arabidopsis proteome. *Nature* **579**, 409–414 (2020).
64. M. Bürger, J. Chory, Stressed out about hormones: How plants orchestrate immunity. *Cell Host Microbe* **26**, 163–172 (2019).
65. G. Bannenberg, M. Martínez, M. Hamberg, C. Castresana, Diversity of the enzymatic activity in the lipoxygenase gene family of Arabidopsis thaliana. *Lipids* **44**, 85–95 (2009).
66. A. Peñaloza-Vázquez, G. M. Preston, A. Collmer, C. L. Bender, Regulatory interactions between the Hrp type III protein secretion system and coronatine biosynthesis in Pseudomonas syringae pv. tomato DC3000. *Microbiology (Reading)* **146**, 2447–2456 (2000).
67. R. Völz *et al*., The Trihelix transcription factor GT2-like 1 (GTL1) promotes salicylic acid metabolism, and regulates bacterial-triggered immunity. *PLoS Genet.* **14**, e1007708 (2018).
68. J. Shin, K. Heidrich, A. Sanchez-Villarreal, J. E. Parker, S. J. Davis, TIME FOR COFFEE represses accumulation of the MYC2 transcription factor to provide time-of-day regulation of jasmonate signaling in Arabidopsis. *Plant Cell* **24**, 2470–2482 (2012).
69. R. Martin-Arevalillo *et al*., Structure of the *Arabidopsis* TOPLESS corepressor provides insight into the evolution of transcriptional repression. *Proc. Natl. Acad. Sci. U.S.A.* **114**, 8107–8112 (2017).
70. N. T. Krogan, K. Hogan, J. A. Long, APETALA2 negatively regulates multiple floral organ identity genes in Arabidopsis by recruiting the co-repressor TOPLESS and the histone deacetylase HDA19. *Development* **139**, 4180–4190 (2012).
71. B. Zou *et al*., The Arabidopsis chromatin-remodeling factor CHR5 regulates plant immune responses and nucleosome occupancy. *Plant Cell Physiol.* **58**, 2202–2216 (2017).
72. Y. Li, M. J. Tessaro, X. Li, Y. Zhang, Regulation of the expression of plant resistance gene SNC1 by a protein with a conserved BAT2 domain. *Plant Physiol.* **153**, 1425–1434 (2010).
73. L. López-González *et al*., Chromatin-dependent repression of the Arabidopsis floral integrator genes involves plant specific PHD-containing proteins. *Plant Cell* **26**, 3922–3938 (2014).
74. F. Pontvianne *et al*., Nucleolin is required for DNA methylation state and the expression of rRNA gene variants in Arabidopsis thaliana. *PLoS Genet.* **6**, e1001225 (2010).
75. P. Wang *et al*., Quantitative phosphoproteomics identifies SnRK2 protein kinase substrates and reveals the effectors of abscisic acid action. *Proc. Natl. Acad. Sci. U.S.A.* **110**, 11205–11210 (2013).
76. D. Vom Endt, M. Soares e Silva, J. W. Kijne, G. Pasquali, J. Memelink, Identification of a bipartite jasmonate-responsive promoter element in the Catharanthus roseus ORCA3 transcription factor gene that interacts specifically with AT-Hook DNA-binding proteins. *Plant Physiol.* **144**, 1680–1689 (2007).
77. D. Lu, T. Wang, S. Persson, B. Mueller-Roeber, J. H. Schippers, Transcriptional control of ROS homeostasis by KUODA1 regulates cell expansion during leaf development. *Nat. Commun.* **5**, 3767 (2014).
78. Y. Zhang, M. J. Tessaro, M. Lassner, X. Li, Knockout analysis of Arabidopsis transcription factors TGA2, TGA5, and TGA6 reveals their redundant and essential roles in systemic acquired resistance. *Plant Cell* **15**, 2647–2653 (2003).
79. A. Djamei, A. Pitzschke, H. Nakagami, I. Rajh, H. Hirt, Trojan horse strategy in agrobacterium transformation: Abusing MAPK defense signaling. *Science* **318**, 453–456 (2007).
80. A. Pitzschke, A. Djamei, M. Teige, H. Hirt, VIP1 response elements mediate mitogen-activated protein kinase 3-induced stress gene expression. *Proc. Natl. Acad. Sci. U.S.A.* **106**, 18414–18419 (2009).
81. H. Nakagami, H. Soukupová, A. Schikora, V. Zárský, H. Hirt, A Mitogen-activated protein kinase kinase kinase mediates reactive oxygen species homeostasis in Arabidopsis. *J. Biol. Chem.* **281**, 38697–38704 (2006).
82. J. Bigeard, N. Rayapuram, L. Bonhomme, H. Hirt, D. Pflieger, Proteomic and phosphoproteomic analyses of chromatin-associated proteins from Arabidopsis thaliana. *Proteomics* **14**, 2141–2155 (2014).
83. M. S. Cline *et al*., Integration of biological networks and gene expression data using Cytoscape. *Nat. Protoc.* **2**, 2366–2382 (2007).
84. T. Tian *et al*., agriGO v2.0: A GO analysis toolkit for the agricultural community, 2017 update. *Nucleic Acids Res.* **45**, W122–W129 (2017).
85. C. M. Hooper *et al*., SUBAcon: A consensus algorithm for unifying the subcellular localization data of the Arabidopsis proteome. *Bioinformatics* **30**, 3356–3364 (2014).
86. C. M. Hooper, I. R. Castleden, S. K. Tanz, N. Aryamanesh, A. H. Millar, SUBA4: The interactive data analysis centre for Arabidopsis subcellular protein locations. *Nucleic Acids Res.* **45**, D1064–D1074 (2017).
87. H. Dinkel *et al*., ELM 2016—Data update and new functionality of the eukaryotic linear motif resource. *Nucleic Acids Res.* **44**, D294–D300 (2016).
88. M. Jarad *et al*., The lamin-like LITTLE NUCLEI 1 (LINC1) regulates pattern-triggered immunity and jasmonic acid signaling. *Front. Plant Sci.* **10**, 1639 (2020).
89. M. Almeida Trapp, G. D. De Souza, E. Rodrigues-Filho, W. Boland, A. Mithöfer, Validated method for phytohormone quantification in plants. *Front. Plant Sci.* **5**, 417 (2014).
90. K. Arnold, L. Bordoli, J. Kopp, T. Schwede, The SWISS-MODEL workspace: A web-based environment for protein structure homology modelling. *Bioinformatics* **22**, 195–201 (2006).
91. J. A. Vizcaíno *et al*., 2016 update of the PRIDE database and its related tools. *Nucleic Acids Res.* **44**, D447–D456 (2016).